Desalination and Water Treatment
www.deswater.com
doi: 10.5004/dwt.2021.27324

228 (2021) 121–132
July

Preparation of a nanoporous composite membrane with excellent antibacterial performance using a metal–organic framework and graphene oxide

Zhiwei Wang[a], Ruidian Su[a], Zhen Liu[a], Yi Chen[a], Baoyu Gao[a], Zhining Wang[a], Qian Li[a,b,*]

[a]*Shandong Key Laboratory of Water Pollution Control and Resource Reuse, School of Environmental Science and Engineering, Shandong University, Qingdao 266200, China, emails: qianli@sdu.edu.cn (Q. Li), 963715092@qq.com (Z. Wang), 1164842217@qq.com (R. Su), 2567058284@qq.com (Z. Liu), 1051386168@qq.com (Y. Chen), baoyugao_sdu@aliyun.com (B. Gao), wangzhn@sdu.edu.cn (Z. Wang)*
[b]*Shenzhen Research Institute of Shandong University, Shenzhen 518057, China*

Received 10 August 2020; Accepted 8 April 2021

ABSTRACT

The surface modification of polyacrylonitrile (PAN) ultrafiltration membranes with advanced porous framework materials is suggested as a directional design of membrane apertures and capabilities to improve their permselectivity and antifouling/antibacterial performance. In this work, a 2D metal–organic framework, HKUST-1, and reduced graphene oxide (rGO) were used to modify a PAN membrane and prepare a novel composite membrane named HKUST-1/rGO/PAN for dye wastewater treatment. X-ray photoelectron spectroscopy, scanning electron microscopy, atomic force microscopy and energy dispersive X-ray spectrometer analyses were used to evaluate the structure and chemical composition of the as-obtained membranes. HKUST-1/rGO/PAN exhibited a pure water flux of 58.46 L m^{-2} h^{-1} bar^{-1}, which was 2.8 times higher than that of an rGO/PAN membrane. The membrane rejection for Methylene blue was more than 90% after 2 h of continuous operation. The composite membrane also exhibited excellent antifouling and antibacterial properties. The removal ratio greatly improved in the antifouling experiment after 3 rounds of sequential fouling and washing, and the inhibition rate against *Escherichia coli* and *Staphylococcus aureus* reached 100%. This work offers a simple technology for exploiting novel multifunctional composite membranes with long-term operational stability and strong antibacterial properties for water treatment.

Keywords: HKUST-1; Reduced graphene oxide; Composite membrane; Dye; Antibacterial

1. Introduction

Membrane separation technology has been applied in many fields because of its easy operation, strong selectivity, low energy consumption, and extensive application [1,2]. However, in the process of liquid separation, the membrane easily breeds bacteria, thus leading to the secondary pollution of products and an increase in energy consumption. For example, *Salmonella* and *Escherichia coli* in water can cause various diseases that have the following symptoms: vomiting, fever, diarrhea, hemolytic anemia acute renal failure or even death [3,4]. It is a key challenge to find efficient methods that can enhance the antibacterial properties of membranes. Currently, many antibacterial substances have been used to modify membranes to improve their antibacterial properties. According to the molecular structure of these antibacterial substances, they can be divided into inorganic antibacterial agents (such as inorganic nanoparticles Ag, Au and Cu, etc.) [5], carbon nanomaterials [6], and organic antibacterial agents (chitosan [7], lysine, quaternary ammonium salts and their copolymers) [8]. Organic

* Corresponding author.

1944-3994/1944-3986 © 2021 Desalination Publications. All rights reserved.

antibacterial agents are mostly used to prepare antibacterial ultrafiltration membranes through blending and surface modifications, which have shortcomings, such as complicated operations while producing a surface with limited antibacterial properties. In comparison, inorganic antibacterial agents, which possess excellent antibacterial efficiency due to the release of metal ions and a simple preparation process, have been increasingly studied. Various types of dopants, such as Ag NPs, TiO_2, Fe NPs, graphene quantum dots, and carbon nanotubes, have displayed excellent potential for eliminating bacterial activity due to their superb antibacterial behavior [9]. However, inorganic antibacterial agents may not be durable and may cause secondary pollution, which limit the antibacterial activity of composite membranes [10].

Recently, metal–organic frameworks (MOFs) have been increasingly studied due to their high potential for wide range of use [11], such as in catalysis [12], separation [13], sensors [14] and drug delivery [15,16]. MOFs composed of metal ions and bridged organic ligands have been introduced into the field of membrane separation due to their special physicochemical properties [17,18]. Yang et al. [19] prepared a composite membrane named ZIF-8/PEI-HPAN that exhibited 99.2% rejection for Congo red solution. In another work, on a polysulfone ultrafiltration support, a new thin nanocomposite membrane was reported by doping MIL-101(Cr) into the dense selective polyamide layer, and the water permeance was increased [20]. However, it is worth noting that there are few reports on preparing antibacterial membranes using MOFs. The antibacterial compounds of MOFs have several superiorities, including broad-spectrum antibacterial properties against gram-negative and gram-positive bacteria with long-lasting persistence, high efficiency and thermal stability [21,22]. Many MOFs have been proposed as excellent antibiofouling candidates. Three different MOFs based on Co (Co-SIM1), Zn (Zn-SIM1) and Ag (Ag-TAZ) caused >50% inhibition towards cyanobacteria [23]. Lu et al. [24] synthesized two novel Ag-based MOFs that slowly released Ag^+ and exhibited excellent antibacterial effects toward both gram-negative bacteria and gram-positive bacteria. The antibacterial activity of MOFs is due to the presence of antimicrobial cations such as Ag^+, Cu^{2+} and Zn^{2+}. In particular, as an endogenous low-toxicity transition metal cation, Cu^{2+} is widely used in antibacterial applications [25]. The metal center of HKUST-1 is copper, and Cu^{2+} and trimesic acid coordinate to form a paddlewheel structure. HKUST-1 has a porous structure with excellent stability, which is good for gas and liquid separation. Herein, HKUST-1 was used to construct a dense layer of membranes on the surface for water separation. However, due to the limited aqueous stability of HKUST-1, it requires a stable skeleton to obtain a stabilized composite membrane. It is known that reduced graphene oxide (rGO) is a two-dimensional material with an atomic-scale thickness, and the two-dimensional nanochannels between adjacent layers can provide a transmission path for small molecules while effectively blocking large-sized molecules [26]. Thus, rGO can form an interpenetrating structure with the MOFs to improve the stability of the selective layer of the membrane that retains macromolecular pollutants [27,28]. Furthermore, the sharp edges of rGO can pierce bacteria synergizing with the MOF for sterilization during water separation [29].

In this paper, we fabricate a novel composite ultrafiltration membrane (HKUST-1/rGO/PAN–polyacrylonitrile) for dye rejection by simple filtration. A schematic illustration of the HKUST-1/rGO membrane is shown in Fig. 1. The permeability and antifouling of the composite membrane are tested for the separation of Methylene blue during filtration. The antibacterial activities against *E. coli* and *Staphylococcus aureus* of the HKUST-1/rGO/PAN membrane are also determined. To the best of our knowledge, this is the first attempt to fabricate a composite membrane with 2D Cu-based MOFs to achieve the triple purpose of separating pollutants while exhibiting antifouling and antibacterial properties during wastewater treatment.

2. Experimental

2.1. Chemicals and materials

Graphite powder, dopamine hydrochloride and tris(hydroxymethyl)aminomethane were provided by Aladdin Bio-Chem Technology Co., Ltd., (Shanghai, China). Copper acetate hydrate ($Cu(CH_3COO)_2{\cdot}H_2O$), trimesic acid (H_3BTC) and Methylene blue (MB) were purchased from Macklin Biochemical Co., Ltd., (Shanghai, China). Hydrochloric acid (HCl), sodium hydroxide (NaOH), sulfuric acid (H_2SO_4), phosphoric acid (H_3PO_4) potassium permanganate ($KMnO_4$), hydrogen peroxide (H_2O_2), N,N-dimethylformamide (DMF), and absolute ethanol (C_2H_5OH) were supplied by Sinopharm Chemical Reagent Co., Ltd., (Shanghai, China). The PAN membrane was purchased from RisingSun Membrane Technology Co., Ltd., (Beijing, China). All reagents were of analytical grade and used without further purification.

2.2. Preparation of HKUST-1, GO and HKUST-1/rGO

2D HKUST-1 was synthesized according to methods reported in the literature [30]. Briefly, 10 mmol of $Cu(CH_3COO)_2{\cdot}H_2O$ and 3.6 mmol of H_3BTC were added to 70 mL of solvent (DMF:ethanol = 4:1), and the mixture

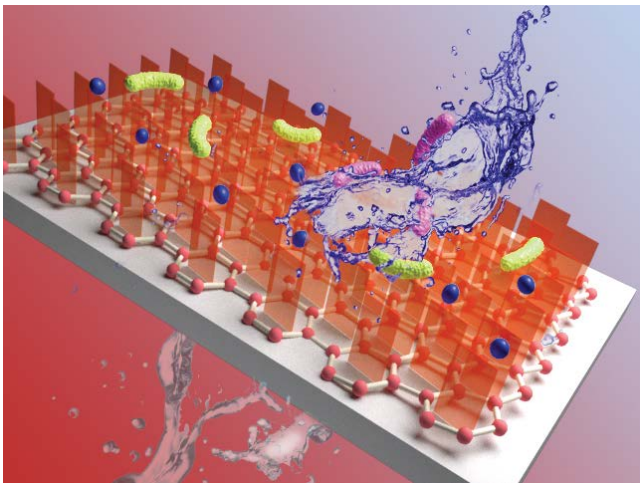

Fig. 1. Schematic illustration of the HKUST-1/rGO membrane.

was sonicated for 1 h. Then, the mixture was transferred to a Teflon-lined autoclave for solvothermal treatment at 393 K for 8 h. After cooling to room temperature, the mixture was centrifuged at 8,000 rpm for 5 min, providing navy blue products that were washed three times using ethanol. Finally, the products were dried at 323 K in a vacuum drying oven.

GO was synthesized according to the Hummers method [31]. Briefly, 360 mL of H_2SO_4 and 40 mL of H_3PO_4 were poured in a 1,000 mL beaker and stirred in a low-temperature reaction bath at 278 K. Then, 3.0 g of graphite and 18.0 g of $KMnO_4$ were slowly added to the mixture. After stirring for 1 h, the mixture was transferred to a water bath at 323 K and stirred for 12 h. Subsequently, 200 g of ice and 8 mL of H_2O_2 were added to the mixture to remove excess $KMnO_4$. Next, the slurry was centrifuged at 10,000 rpm for 10 min, and the solid was washed with deionized water until the pH was neutral. Finally, graphene oxide was obtained after freeze-drying.

The obtained graphene oxide was dispersed in 25 mL of ultrapure water, and after adding HKUST-1, the mixture was stirred and ultrasonicated for 2 h. Then, 0.05 g of dopamine hydrochloride was added, and the pH was adjusted to 8.5 with Tris-HCl. Next, the mixture was transferred to a flask and stirred at 70°C for 24 h. Finally, the HKUST-1/rGO casting solution was cooled to room temperature for further use.

2.3. Synthesis of the composite membranes

The PAN membranes were soaked in ethanol and ultrapure water for 24 h. Then, 0.5 mL of the casting solution was diluted to 50 times the original concentration and filtered onto the surface of the PAN membrane at 0.09 MPa. The prepared membranes were named M0, M40, M80, M120 and M160 to express the different doses (Table 1). Finally, the membranes were dried at 323 K for 20 min.

2.4. Characterization

Scanning electron microscopy (SEM, Hitachi S-4800) was used to detect the morphology of the materials and the surface and cross-section morphologies of the membranes. The crystalline structure of the materials and membranes was investigated by X-ray diffraction (XRD, Ultima IV, 10°C/min). The surface chemical composition was determined by X-ray photoelectron spectroscopy (XPS; Thermo ESCALAB 250Xi). The surface roughness and three-dimensional images of the membranes were characterized by atomic force microscopy (AFM; NanoWizard 4, America).

Table 1
Compositions of the composite membranes in this study

Composite membrane	M0	M40	M80	M120	M160
HKUST-1 (mg/L)	0.0	40.0	80.0	120.0	160.0
GO (mg)	1.25	1.25	1.25	1.25	1.25
PDA (mg)	0.5	0.5	0.5	0.5	0.5

A NETZSCH STA 449 F5 instrument was applied to obtain the thermogravimetric analysis (TGA) in flowing air and N_2 at a heating rate of 10°C/min. The hydrophilicity of the membranes was measured by a dynamic contact angle analyzer (JY-82B Kruss DSA) using 1.5 mL of UP-water as the liquid drop each time.

2.5. Performance evaluation

The separation test of the composite membranes was evaluated by a Methylene blue aqueous solution in vacuum filtration equipment at room temperature (20°C–25°C). A steady water flux was ensured for each membrane by precompacting at 0.9 bar for 20 min.

The permeate flux (J_w, L m^{-2} h^{-1}) was calculated by measuring the permeate volume (ΔV, L) through the effective area of the membrane (A_m, m^2) at a certain time (Δt, h). Solute rejection (R, %) was evaluated by measuring the MB concentrations of the permeate (C_p) and feed (C_f) solution using a UV spectrophotometer at 664 nm. The effective area of all solutions permeating the membrane was 12.56 cm^2 (A_m, m^2).

$$J_w = \frac{\Delta V}{\left(A_m \times \Delta t\right)} \tag{1}$$

$$R = \frac{C_f - C_p}{C_f} \times 100\% \tag{2}$$

In addition, the test was carried out for 2 h to evaluate the long-term stability of membranes using the same vacuum filtration system at an operation pressure of 0.9 bar. Water samples were collected at 20 min intervals for recording the water flux and MB rejection.

The antifouling property of a membrane has a significant influence on its practical application. To evaluate this property of the membrane, the rGO/PAN and HKUST-1/rGO/PAN membranes were used to adsorb MB three ti1ter adsorption of a 20 mL MB solution (30 mg/L), a 1% HCl and ethanol solution was used to wash the membrane for 40 min. The flux recovery ratio (FRR) and repeat removal rate (R1, R2, and R3) were measured. The R1, R2, and R3 formulas are the same as Eq. (2), and the FRR formula is as follows:

$$\mathrm{FRR} = \frac{J_R}{J_0} \times 100\% \tag{3}$$

where J_R and J_0 represent the first and second fluxes, respectively.

To investigate the antibacterial properties of the composites, rGO and HKUST-1/rGO were tested against *E. coli* and *S. aureus*, respectively. First, *E. coli* and *S. aureus* suspensions at a concentration of ~1.0 × 10^6 cfu/mL were prepared. Next, 1 mL of bacterial solution and material were transferred into 20 mL of sterile physiological saline. Then, the mixture was shaken in a constant-temperature

shaking incubator at 37°C for 2 h to allow the bacteria to fully contact the sample. Finally, 0.1 mL of the bacterial suspension was taken and uniformly coated on an LB solid medium plate and placed in a 37°C incubator for 12 h. The bacterial killing ratio (R_k) of the material was calculated using Eq. (4):

$$R_k = \frac{N_B - N_S}{N_B} \times 100\% \quad (4)$$

where N_B is the number of live bacterial colonies on the reference plate, and N_S is the total number of live bacterial colonies on the sample plate. The photograph of bacterial colonies after the inoculation of *E. coli* and *S. aureus* with materials were named Blank-E, rGO-E, HKUST-1/rGO-E for *E. coli* and Blank-S, rGO-S and HKUST-1/rGO-S for *S. aureus*.

To observe the antibacterial properties of the composite membrane, M0 and M120 were tested against *E. coli* and *S. aureus*. First, *E. coli* and *S. aureus* suspensions were prepared at a concentration of ~1.0 × 10^6 cfu/mL. Second, 1 mL of the bacterial solution was transferred to 20 mL of sterile physiological saline containing a membrane with a 4 cm diameter, which was then placed in a constant-temperature shaking incubator at 37°C for 2 h. Next, each membrane was rinsed with 5 mL of physiological saline, and the solution was placed in a 100 mL beaker and cultivated in a 37°C constant temperature shaking incubator. After 10 min, 0.1 mL of the bacterial suspension was taken and uniformly coated on a sterile LB solid medium plate. Then, the coated plates were placed in a 37°C incubator for 12 h. In this experiment, PAN membranes were used as a blank. Photographs of the bacterial colonies after the inoculation of *E. coli* and *S. aureus* with the membranes were named PAN-E, M0-E, M120-E, PAN-S, M0-S and M120-S, respectively.

A live/dead assay was also used to test the bacterial viability after contacting the prepared membranes using a LIVE/DEAD BacLight bacterial viability kit containing calcein-AM/PI fluorescent staining agents. First, the *E. coli* and *S. aureus* suspensions were prepared at a concentration of ~1.0 × 10^6 cfu/mL. Second, 1 mL of the bacterial solution was transferred to 20 mL of sterile physiological saline containing a membrane with a 4 cm diameter, which was then placed in a constant-temperature shaking incubator at 37°C for 2 h. Then, 1 mL of the supernatant of the membranes was stained at room temperature in the dark for 15 min. Next, the supernatant was transferred to a glass slide and observed with a laser scanning confocal microscope (OLYMPUS CX31, China). With an appropriate mixture of the fluorescent staining agent calcein-AM and propidium iodide, bacteria with intact cell membranes were stained fluorescent green, and bacteria with damaged cell membranes were stained fluorescent red [7].

To detect whether the concentration of ions in the water caused secondary pollution. The release of copper ions from the membranes was monitored via batch experiments by atomic absorption spectrometry.

3. Results and discussion

3.1. Evaluating the physiochemical properties of the materials and composite membranes

The morphology of the materials was characterized by SEM and is displayed in Fig. 2a–c. The SEM images suggested that rGO had a flake-like structure with stacked fragments (Fig. 2a) and that HKUST-1 exhibited an irregular microflower shape (Fig. 2b). The morphology of the HKUST-1/rGO materials is displayed in Fig. 2c, suggesting that many ravines are formed on the surface of the composite material, which can provide additional paths for water molecules. The XRD spectra of HKUST-1 and GO exhibited typical diffraction peaks (Fig. 2d). The sharp peak at 9.42° corresponded to GO, and the typical diffraction peaks at 6.68°, 9.44°, 11.52° and 13.3° were assigned to HKUST-1. The peaks at 36.34° and 38.96° represented Cu_2O and CuO, respectively, in the XRD pattern of HKUST-1 [32]. XPS analysis was carried out to assess the elemental composition and chemical variations of HKUST-1/rGO and rGO, as shown in Fig. 2e–j. As described in Fig. 2e, the energy peaks of HKUST-1/rGO and rGO were predominantly composed of C, O, N, and the spectra of HKUST-1/rGO presented a new signal assigned to the presence of copper (HKUST-1). The result of the C 1s self-evident spectra of rGO (Fig. 2f) showed two typical peaks: a primary peak corresponding to the C–O bond located at 286.3 eV and another peak at 284.8 eV conforming to C–C or C=C bonds [33]. The enhanced intensity of the C–O peak in HKUST-1/rGO was consistent with the existence of the free –COOH functional group of the H_3BTC ligand in HKUST-1 (Fig. 2g). Additionally, the N 1s spectrum of rGO (Fig. 2h) exhibited three peaks: a major peak attributed to the =N–R bond located at 399.7 eV, a middle peak at 401.5 eV attributed to the R–NH–R bond and a small peak at 406.8 eV corresponding to the R–NH_2 bond [34]. The improved intensity of the =N–R peak in HKUST-1/rGO was attributed to the presence of –NH_3–COO (Fig. 2i), which was due to the combination of the –NH_3^+ in dopamine molecules with the –COO^- in the H_3BTC ligand. The shape of the new copper signals illustrated the existence of HKUST-1 in HKUST-1/rGO (Fig. 2j). The peaks of Cu^{2+} were situated at 954.7 and 934.68 eV, and the peaks at 952.8 and 932.9 eV were separately assigned to Cu $2p_{1/2}$ and Cu $2p_{3/2}$, respectively [35].

The surface and cross-sectional morphology of the membranes are shown in Figs. 3a–c. The rGO/PAN membrane exhibits a flat and dense surface with obvious nodule granule features, which is the characteristic morphology of composite membranes formed by the stack of flaky rGO (Fig. 3a). After the addition of HKUST-1, some irregular microflower structures were observed, and the active layer covered the surface of HKUST-1/rGO/PAN (Fig. 3b and c). Additionally, the energy dispersive X-ray spectroscopy mapping clearly validated that copper from HKUST-1 was distributed on the surface and in the channels of HKUST-1/rGO/PAN. The XRD spectra (Fig. 3d) of the HKUST-1/rGO/PAN and rGO/PAN membranes exhibited no significant changes because the peaks of HKUST-1 and rGO were covered by the peaks

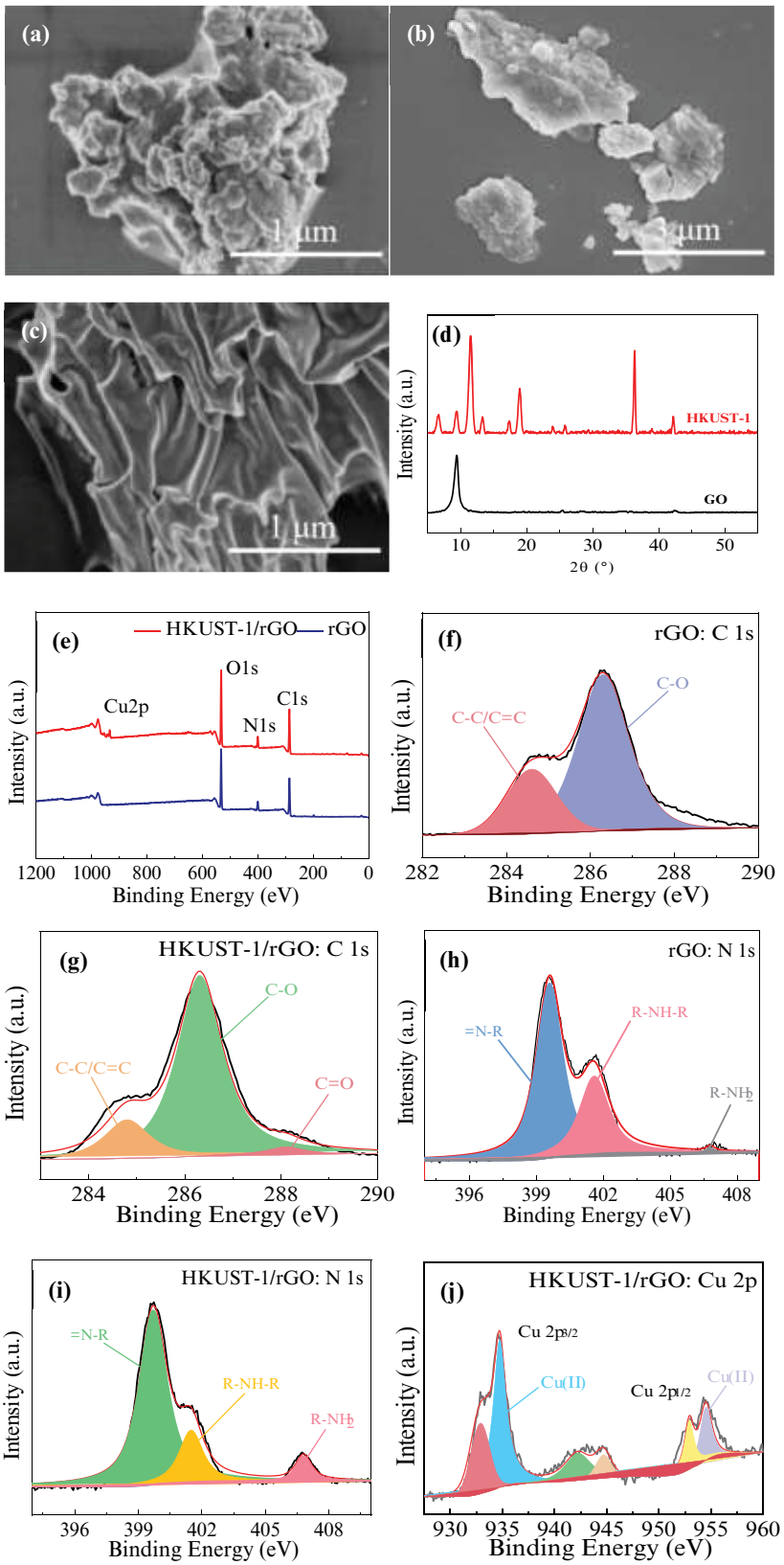

Fig. 2. Characterization results of the materials. SEM images of (a) rGO, (b) HKUST-1, and (c) HKUST-1/rGO; (d) XRD spectra of the materials. XPS survey spectra of the composite materials: (e) HKUST-1/rGO and rGO, (f) C 1s spectra for rGO, (g) C 1s spectra for HKUST-1/rGO, (h) N 1s spectra for rGO, (i) N 1s spectra for HKUST-1/rGO and (j) Cu 2p spectra for HKUST-1/rGO.

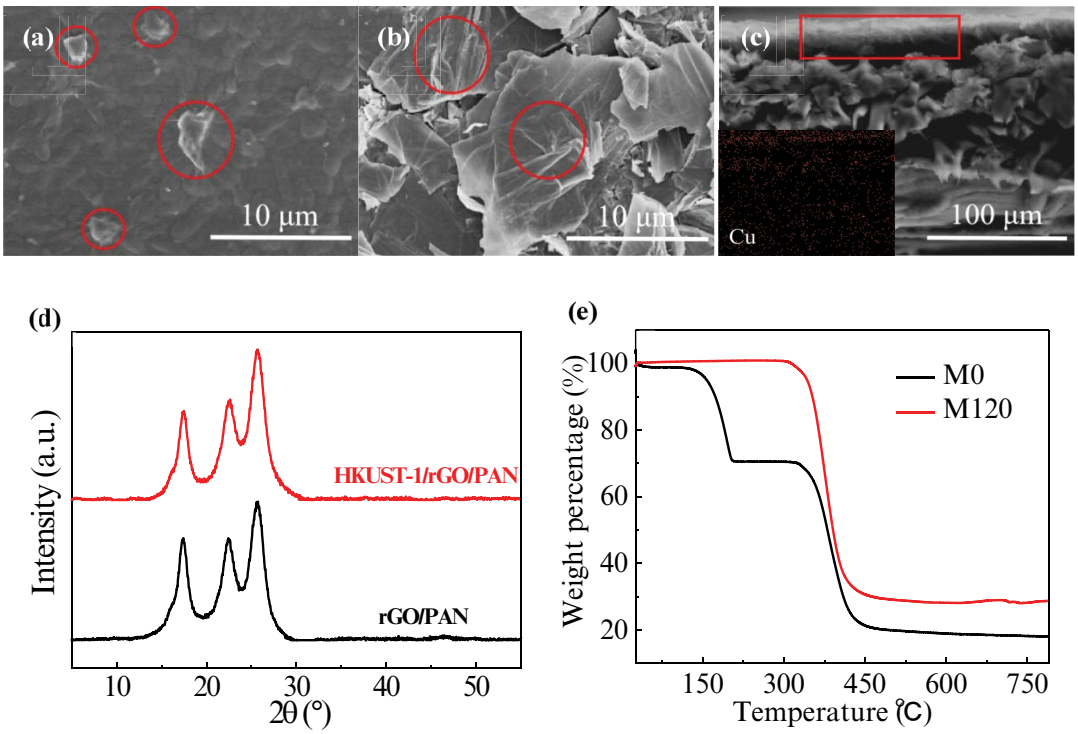

Fig. 3. Characterization results of the membranes. SEM surface images of (a) rGO/PAN and (b) HKUST-1/rGO/PAN. (c) SEM cross-section and energy dispersive X-ray spectroscopy image of HKUST-1/rGO/PAN, (d) XRD spectrum of the membranes and (e) TGA curves of M0 and M120.

of the PAN membrane. As shown in Fig. 3e, the curve of M0 attained a plateau up to 130°C without any obvious mass loss, demonstrating the framework integrity during this process. Then, M0 showed a continuous weight loss from 130°C to 200°C caused by the sublimation of residual dimethylamide. From 200°C–300°C, there was no obvious weight loss, indicating the stability of M0 in this temperature range. The apparent weight loss of 50% in the second part that occurred from 300°C to 450°C was assigned to the collapse in the structure of the sample [36]. In this process, large amounts of CO_2, CO, CH_4, HCN, NH_3 were released along with the decomposition of the membrane and the collapse of the rGO structure. Additionally, there was no significant weight loss in the M120 curve from 25°C–300°C, indicating that HKUST-1 improved the thermal stability of the composite membrane. From 300°C–450°C, the weight of M120 decreased by 70%, and the structure of the sample collapsed completely near 450°C, which was consistent with literature reports. In this process, with the decomposition of M120 and the release of a large amount of gas, cuprous oxide and copper oxide were produced at the same time [37].

As shown in Fig. 4, an AFM surface analysis was conducted to further explore the surface morphology of the membranes with different concentrations of HKUST-1. The AFM parameters in terms of height, R_a and R_q are illustrated in Fig. 4f. It can be clearly seen that the height and roughness parameters of the membrane increased after the formation of HKUST-1/rGO on the surface. However, the more pronounced ridge and valley morphology of the membranes decreased with an increasing concentration of HKUST-1. Additionally, the R_a, R_Q and height of the membranes first increased, then clearly decreased, before increasing one more time at 160 mg/L MOFs due to the deposition of HKUST-1 on the surface. On account of the addition of MOFs, the space between rGO sheets was first expanded by HKUST-1, resulting in an increase in surface roughness and height. Then, HKUST-1 filled and leveled the gaps on the surface, leading to a flat surface with reduced roughness and height. Notably, the rough surface morphology may possibly lower the fouling tendency of the functional membrane. Therefore, 120 mg/L HKUST-1 (M120) was determined to be a favorable concentration for further experiments.

The water contact angle was measured as the degree of hydrophilicity of the membrane surface, which plays an important role in its pure water flux and antifouling performance. According to Fig. 5, the water contact angle of the PAN membrane was approximately 78.6°. As can be observed, M0 had a larger water contact angle and therefore lower hydrophilicity than the neat PAN membrane due to the hydrophobic nature of the incorporated rGO nanoparticles on the membrane surface. After the incorporation of the MOF, the water contact angle of M120 decreased and reached a lower value of 69.3°, which can be related to the presence of abundant hydroxyl groups on the structure of HKUST-1 (Fig. 5c).

3.2. Performance evaluation of the membranes

The water flux and MB rejection of the composite membranes are evaluated in Fig. 6. The water flux steadily increased from 20.51 to 58.46 L m^{-2} h^{-1} (LMH)

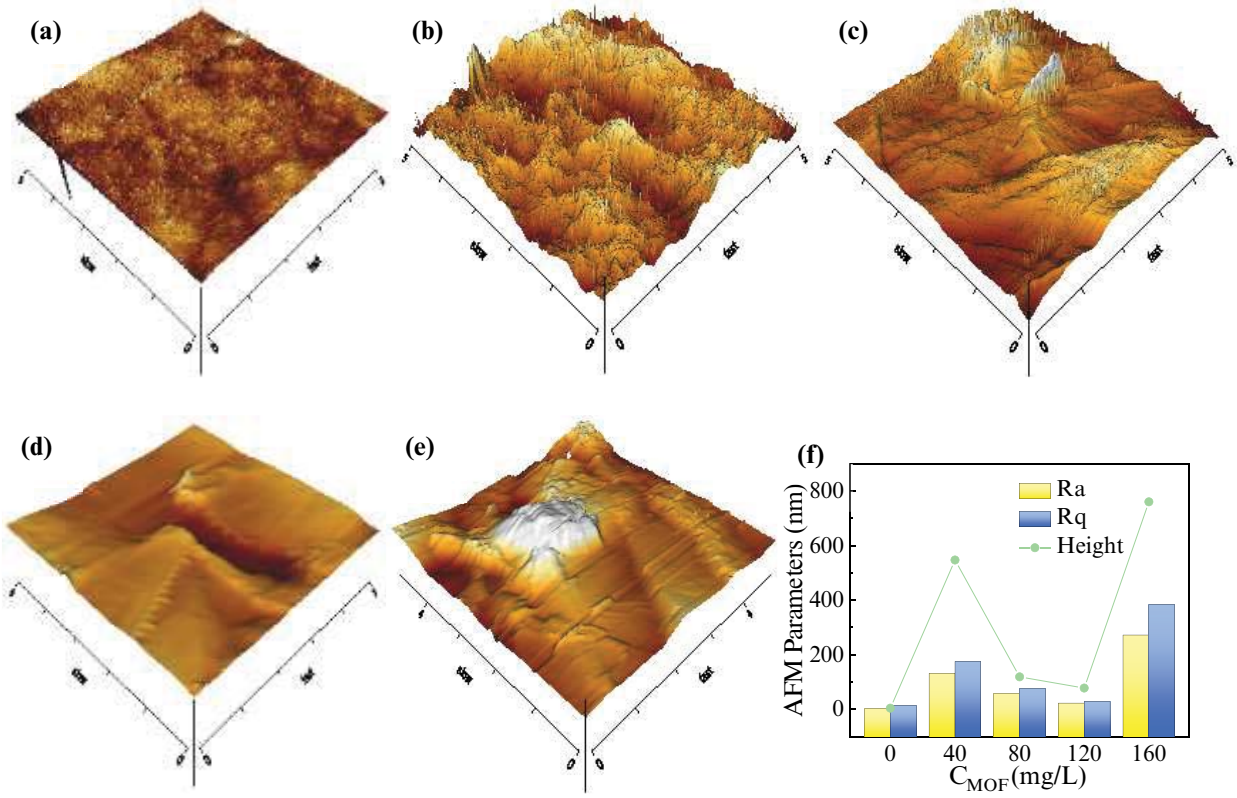

Fig. 4. AFM 3D images and roughness parameters of membranes at different concentrations of HKUST-1: (a) 0, (b) 40, (c) 80, (d) 120 and (e) 160 mg/mL. (f) AFM parameters of the membranes with different concentrations of HKUST-1.

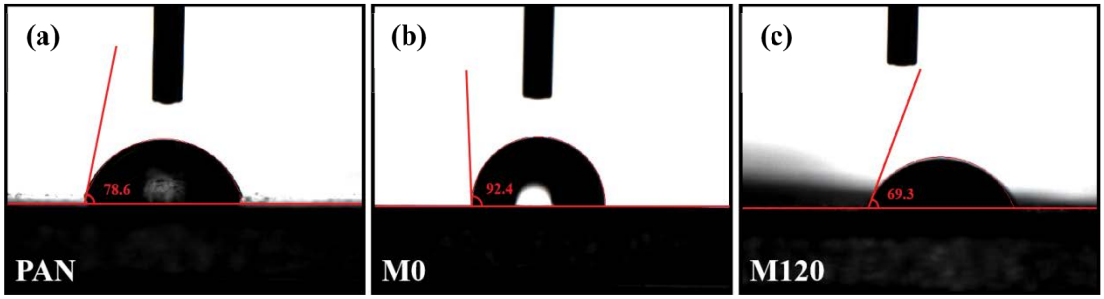

Fig. 5. Contact angles of the different membranes: (a) PAN, (b) M0, and (c) M120.

with an increasing HKUST-1 from 0 to 120 mg/L and then decreased to 52.39 L m^{-2} h^{-1} at 160 mg/L. This clear change in flux can be due to five possible reasons. First, the surface hydrophilicity of the HKUST-1/rGO/PAN membranes was improved by the addition of MOFs with hydrophilic ligands. Second, the addition of HKUST-1 broke down the intermolecular forces, and hydrogen bonds between the rGO sheet and some voids were unavoidably generated. Third, the relatively flat membrane surface shortened the path of water molecules through the membranes. Fourth, the nanochannels of the MOFs could supply extra water pathways, improving the permeation of water molecules. Fifth, blocking on the membrane surface, due to excess MOFs, caused the flux to decrease. MB rejection of the composite membranes remained at a high level (>90%) with an increasing HKUST-1 loading from 0 to 160 mg/L. The reason for this result is that with an increasing content of MOF in the selective layer, the structure of the active layer became more stable, and the water penetration into the membrane increased due to the decreased mass transfer resistance for water molecules. From the above results, the HKUST-1/rGO/PAN membrane had better performance in regard to MB rejection than rGO/PAN membranes.

In ultrafiltration systems, long-term performance is important in regard to membrane performance characteristics. Thus, the rGO/PAN and HKUST-1/rGO/PAN membranes were tested for 120 min of continuous operation, and the results are demonstrated in Fig. 6c–d. Regarding the rGO/PAN membrane, both water permeability and MB rejection decreased as the operating time

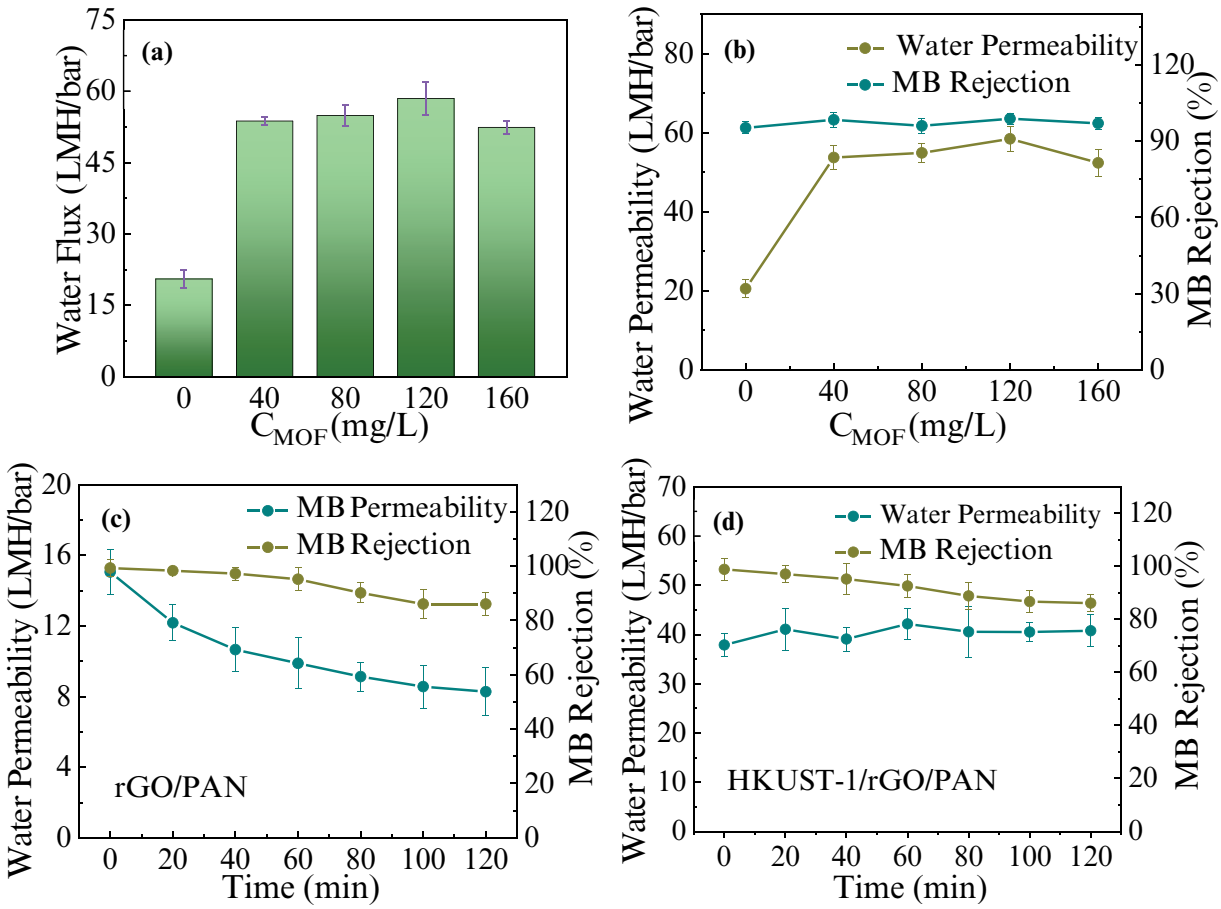

Fig. 6. (a) Pure water flux, (b) MB flux and rejection with different concentrations of HKUST-1, and the separation performance of the (c) rGO/PAN and (d) HKUST-1/rGO/PAN membranes.

increased. However, regarding the HKUST-1/rGO/PAN membrane, the addition of MOFs resulted in a slight decrease in MB rejection, while the water permeability increased by more than 3 times. This result demonstrated that the HKUST-1/rGO/PAN membrane with a firm active layer was available for long-term operation.

3.3. Antifouling performance of the membranes

To evaluate the antifouling capacity of the membranes, the removal ratio during the antifouling tests was observed; these tests included 3 rounds of sequential fouling and washing. Fig. 7a and b illustrate the variations in MB flux and rejection during the 3 rounds. As filtration proceeded, the aggregation of rGO caused a large number of defects in the membrane, which resulted in a decrease in MB rejection. After the addition of MOFs, the MB rejection of HKUST-1/rGO/PAN clearly improved compared with that of rGO/PAN, and M120 containing 120 mg/L HKUST-1 exhibited the highest FRR. This result demonstrated that HKUST-1-functionalized membranes exhibited much higher antifouling properties. HKUST-1 improved the hydrophilicity of membranes, which was conducive to the formation of water layers on the membrane surface by adsorbing water molecules. The water layer would prevent dye molecules from adsorbing on the membranes [33]. Moreover, the addition of HKUST-1 in the active layers could prevent the accumulation of dye molecules on the membrane surface, demonstrating that the HKUST-1/rGO/PAN membrane had better recyclability and antifouling performance.

3.4. Antibacterial performance

The antibacterial activity of the composite membranes was evaluated by using two typical gram-negative and gram-positive bacteria. The results of the antibacterial experiments for materials and membranes are shown in Fig. 8. The bacterial killing ratio (R_k) of rGO for *E. coli* and *S. aureus* was 13.03% and 37.28%, respectively, while HKUST-1/rGO significantly increased the R_k of *E. coli* (R_k = 100%) and *S. aureus* (R_k = 76.62%). Clearly, regarding HKUST-1/rGO, the presence of HKUST-1 played an important role in improving the bactericidal properties. Furthermore, the R_k of M0 and M120 were tested and compared with those of the PAN membrane. As shown in Fig. 8f and g, a large quantity of *E. coli* and *S. aureus* strains lived on the PAN membrane surface. In contrast, the viable bacteria observed on the M0 surface decreased, and the bacterial mortality of *E. coli* and *S. aureus* was 13.64%

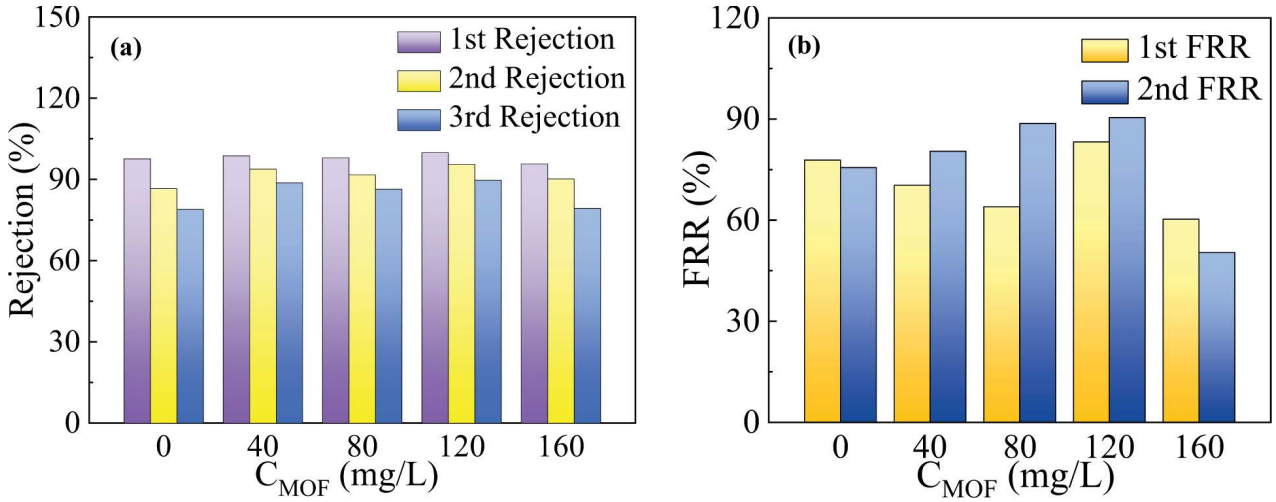

Fig. 7. (a) Rejection and the (b) FRR of the membranes with different HKUST-1 concentrations after three fouling-washing cycles with MB.

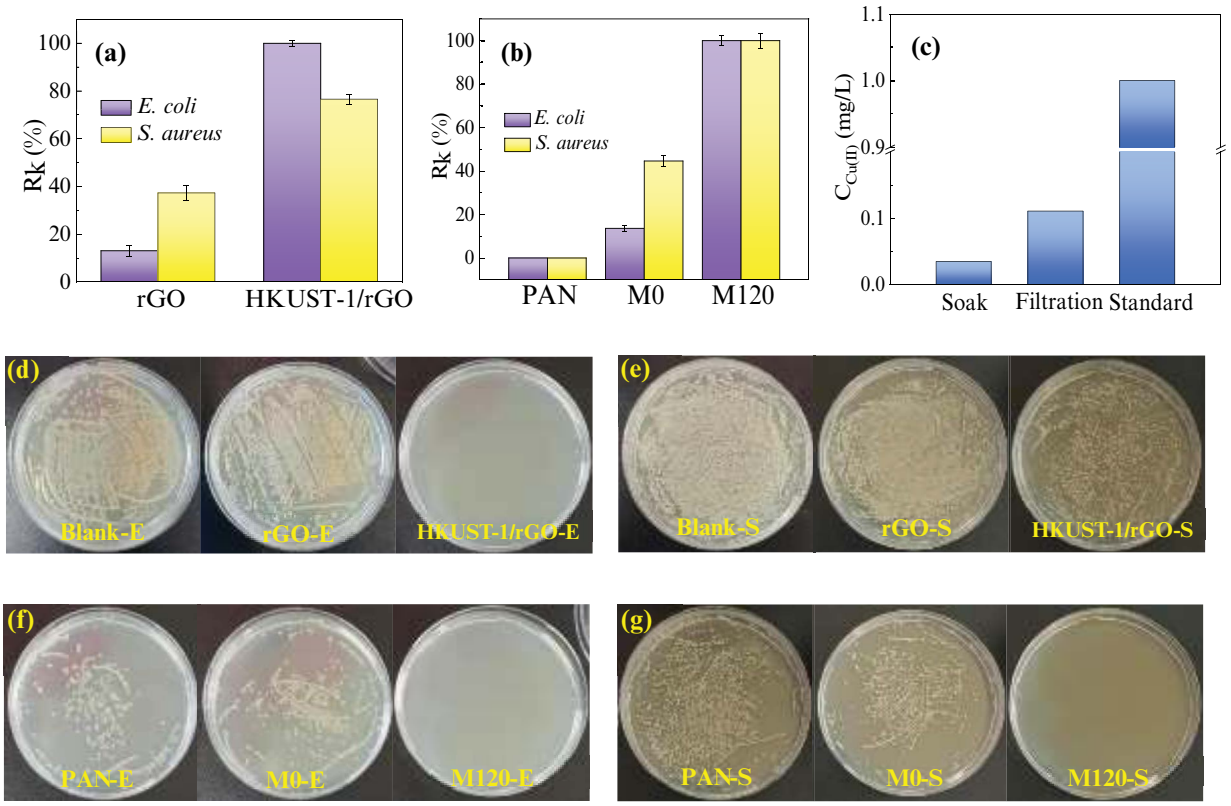

Fig. 8. (a) Antibacterial properties of the materials. (b) Antibacterial properties of the membranes. (c) Release of copper ions in water. (d) Photographs of the bacterial colonies after the inoculation of *Escherichia coli* on the materials. (e) Photographs of the bacterial colonies after the inoculation of *Staphylococcus aureus* on the materials. (f) Photographs of bacterial colonies after the inoculation of *Escherichia coli* on the membranes. (g) Photographs of bacterial colonies after the inoculation of *Staphylococcus aureus* on the membranes.

and 44.63%, respectively. Additionally, colony growth was inhibited on the surface of M120, and the bacterial mortality was approximately 100%. This result was indicative of the antibacterial property of the HKUST-1-functionalized membrane against gram-negative and gram-positive bacteria.

The antibacterial mechanism of membranes included the following pathways. The reasons for the good antibacterial performance were that rGO and HKUST-1 acted similarly to a "spear and shield"; the sharp edges of rGO pierced the bacterial cell membrane by direct adherence. Then, HKUST-1 released Cu^{2+}, which could penetrate

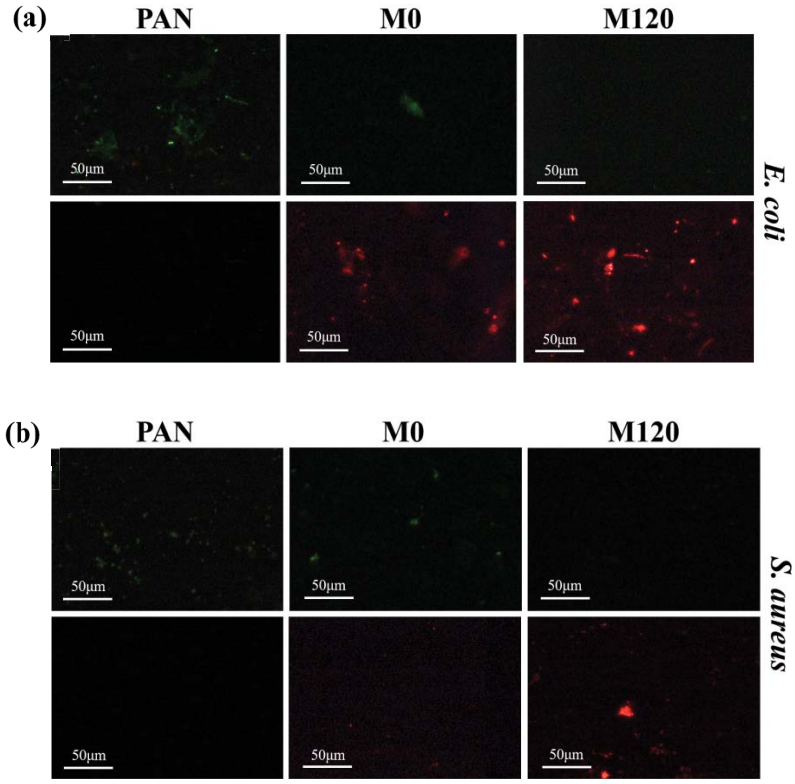

Fig. 9. (a) Live/dead fluorescence images of *Escherichia coli* after exposure to the composite membranes. (b) Live/dead fluorescence images of *Staphylococcus aureus* after exposure to the composite membranes.

Table 2 Comparison of the antibacterial capacities of reported membranes

Antibacterial agent	Antibacterial methods	Bacteria	Antibacterial performance
Phosphorylcholine (PC)-containing polymers [40]	Control cellular adhesion	*Escherichia coli*	90% (Anti-adhesion rate)
2-Methacryloyloxyethyl phosphorylcholine polymers [41]	Control cellular adhesion	*Staphylococcus aureus*, *Streptococcus mutans*, *Pseudomonas aeruginosa*, and *Candida albicans*	95% (Anti-adhesion rate)
Ag-MOFs [42]	Release metal ions	*Escherichia coli* and *Staphylococcus aureus*	Almost 100%
GO-PDA-PEI [43]	Near infrared (NIR) laser irradiation	*Escherichia coli* and *Staphylococcus aureus*	99%
HKUST-1/rGO/PAN (this work)	Release metal ions and contact sterilization	*Escherichia coli* and *Staphylococcus aureus*	Almost 100%

into the bacterial cell, and carboxylic acids in the trimeric acid linker accelerated and promoted the sterilization process [38]. Since rGO and HKUST-1 were available in the active layer of the membrane, they conveniently provided direct contact with bacterial cells and improved antibacterial performance [32]. Furthermore, HKUST-1, which possessed properly distributed metal active sites in its matrix, could act as a reservoir of copper ions to continuously release Cu^{2+}, thus creating sustainable antibacterial activity [39].

Additionally, the release of Cu^{2+} was monitored in both soak and filtration solutions. Fig. 8c shows that the highest Cu^{2+} concentrations detected in the soak and filtration solutions are 0.035 and 0.111 mg/L, respectively, which are far below the maximum contamination extent of Cu in drinking water as reported by the Sanitary Standard for Drinking Water (GB5749-2006) (China). Thus, the release of Cu^{2+} during the operation of the composite membrane could not cause secondary contamination in either the soak or filtration solutions.

Furthermore, a fluorescence test (Fig. 9) was conducted to confirm the bactericidal performance of the membrane. Many green spots and very few red spots appeared in the fluorescence images of the samples in contact with the PAN membrane, indicating that almost no *E. coli* or *S. aureus* were sterilized. After cultivation with M0, many of the bacterial cells were stained red by SYTO PI, revealing that some cells might be disrupted. Almost all the bacteria were stained red upon M120 exposure, which showed that M120 caused noticeable damage to both bacteria owing to its synergistic antibacterial effect.

A comparison of the antibacterial methods and performance of the as-prepared composite membrane with other antibacterial agents are presented in Table 2. Due to the synergistic effect of both rGO and copper ions in HKUST-1, HKUST-1/rGO/PAN exhibited excellent antibacterial performance, indicating its outstanding application potential in water treatment.

4. Conclusion

In this study, rGO and HKUST-1 were loaded onto a PAN membrane using polydopamine by simple filtration to prepare a new composite membrane (HKUST-1/rGO/PAN). The composite membrane possessed excellent water permeability, dye separation and antifouling properties during long-term operation. Bacterial experiments showed that the antibacterial activity of the composite membrane loaded with HKUST-1/rGO reached 100%, which was attributed to the synergistic effect of both rGO and copper ions released from HKUST-1. This work provides a simple method for the preparation of two-dimensional material-based composite membranes, which can not only separate dyes effectively but also release low concentrations of metal ions to improve the antimicrobial performance of the membrane.

Acknowledgement

This work was supported by the National Natural Science Foundation of China (U1906221 and 52070121). This work was also supported by grants from the Major Program of Shandong Province Technological Innovation Project (No. 2020CXGC011403) and Guangdong Basic and Applied Basic Research Foundation (2020A1515011400).

References

[1] S. Lee, J. Choi, Y.-G. Park, H. Shon, C.H. Ahn, S.-H. Kim, Hybrid desalination processes for beneficial use of reverse osmosis brine: current status and future prospects, Desalination, 454 (2019) 104–111.
[2] H. Wang, X. Huang, B. Li, J. Gao, Facile preparation of super-hydrophobic nanofibrous membrane for oil/water separation in a harsh environment, J. Mater. Sci., 53 (2018) 10111–10121.
[3] X. He, D. Yang, X. Zhang, M. Liu, Z. Kang, C. Lin, N. Jia, R. Luque, Waste eggshell membrane-templated CuO-ZnO nanocomposites with enhanced adsorption, catalysis and antibacterial properties for water purification, Chem. Eng. J., 369 (2019) 621–633.
[4] V. Kochkodan, N. Hilal, A comprehensive review on surface modified polymer membranes for biofouling mitigation, Desalination, 356 (2015) 187–207.
[5] X. Yue, T. Zhang, D. Yang, F. Qiu, Z. Li, G. Wei, Y. Qiao, Ag nanoparticles coated cellulose membrane with high infrared reflection, breathability and antibacterial property for human thermal insulation, J. Colloid Interface Sci., 535 (2019) 363–370.
[6] Q. Wu, G.E. Chen, W.G. Sun, Z.L. Xu, Y.F. Kong, X.P. Zheng, S.J. Xu, Bio-inspired GO-Ag/PVDF/F127 membrane with improved anti-fouling for natural organic matter (NOM) resistance, Chem. Eng. J., 313 (2017) 450–460.
[7] C. Wang, J. Fan, R. Xu, L. Zhang, S. Zhong, W. Wang, D. Yu, Quaternary ammonium chitosan/polyvinyl alcohol composites prepared by electrospinning with high antibacterial properties and filtration efficiency, J. Mater. Sci., 54 (2019) 12522–12532.
[8] Z. Li, W. Hu, Y. Zhao, L. Ren, X. Yuan, Integrated antibacterial and antifouling surfaces via cross-linking chitosan-g-eugenol/zwitterionic copolymer on electrospun membranes, Colloids Surf., B, 169 (2018) 151–159.
[9] Y.N. Slavin, J. Asnis, U.O. Häfeli, H. Bach, Metal nanoparticles: understanding the mechanisms behind antibacterial activity, J. Nanobiotechnol., 15 (2017) 65–85.
[10] Z. Wang, Z. Wu, M. Chen, X. Zhang, Y. Wen, Characterization of antibiofouling behaviors of PVDF membrane modified by quaternary ammonium compound – combined use of QCM-D, FCM, and CLSM, J. Water Reuse Desal., 9 (2019) 18–30.
[11] Y. Liu, X. Chen, Y. Yang, Y. Feng, D. Wu, S. Mao, Activation of persulfate with metal–organic framework-derived nitrogen-doped porous Co@C nanoboxes for highly efficient p-chloroaniline removal, Chem. Eng. J., 358 (2019) 408–418.
[12] G. Gao, Q. Xi, Y. Zhang, M. Jin, Y. Zhao, C. Wu, H. Zhou, P. Guo, J. Xu, Atomic-scale engineering of MOF array confined Au nanoclusters for enhanced heterogeneous catalysis, Nanoscale, 11 (2019) 1169–1176.
[13] J. Duan, Y. Pan, G. Liu, W. Jin, Metal-organic framework adsorbents and membranes for separation applications, Curr. Opin. Chem. Eng., 20 (2018) 122–131.
[14] R. Zhang, D. Zhang, Y. Yao, Q. Zhang, Y. Xu, Y. Wu, H. Yu, G. Lu, Metal-organic framework crystal-assembled optical sensors for chemical vapors: effects of crystal sizes and missing-linker defects on sensing performances, ACS Appl. Mater. Interfaces, 11 (2019) 21010–21017.
[15] S. Shalini, S. Komal, R. Indrajit, Magnetic nanoscale metal–organic frameworks for magnetically aided drug delivery and photodynamic therapy, New J. Chem., 41 (2017) 11860–11866.
[16] C. Lin, H. He, Y. Zhang, M. Xu, F. Tian, L. Li, Y. Wang, Acetaldehyde-modified-cystine functionalized Zr-MOFs for pH/GSH dual-responsive drug delivery and selective visualization of GSH in living cells, RSC Adv., 10 (2020) 3084–3091.
[17] D. Huang, X. Wu, J. Tian, X. Wang, Z. Zhou, D. Li, Assembling of a novel 3D Ag(I)-MOFs with mixed ligands tactics: syntheses, crystal structure and catalytic degradation of nitrophenol, Chin. Chem. Lett., 29 (2018) 845–848.
[18] J.L. Harding, J.M. Metz, M.M. Reynolds, A Tunable, Stable, and Bioactive MOF catalyst for generating a localized therapeutic from endogenous sources, Adv. Funct. Mater., 24 (2014) 7503–7509.
[19] L. Yang, Z. Wang, J. Zhang, Highly permeable zeolite imidazolate framework composite membranes fabricated via a chelation-assisted interfacial reaction, J. Mater. Chem. A, 5 (2017) 15342–15355.
[20] Y. Xu, X. Gao, X. Wang, Q. Wang, Z. Ji, X. Wang, T. Wu, C. Gao, Highly and stably water permeable thin film nanocomposite membranes doped with MIL-101 (Cr) nanoparticles for reverse osmosis application, Materials (Basel), 9 (2016) 870–884.
[21] J.H. Jo, H.C. Kim, S. Huh, Y. Kim, D.N. Lee, Antibacterial activities of Cu-MOFs containing glutarates and bipyridyl ligands, Dalton Trans., 48 (2019) 8084–8093.
[22] G. Ximing, G. Bin, W. Yuanlin, G. Shuanghong, Preparation of spherical metal-organic frameworks encapsulating ag nanoparticles and study on its antibacterial activity, Mater. Sci. Eng. C, 80 (2017) 698–707.

[23] K.M. Betancor, S. Aguado, I.R. Palomares, M.T. Belda, F. Leganés, R. Rosal, F. Fernández-Piñas, Co, Zn and Ag-MOFs evaluation as biocidal materials towards photosynthetic organisms, Sci. Total Environ., 595 (2017) 547–555.
[24] X. Lu, J. Ye, D. Zhang, R. Xie, R.F. Bogale, Y. Sun, L. Zhao, Q. Zhao, G. Ning, Silver carboxylate metal-organic frameworks with highly antibacterial activity and biocompatibility, J. Inorg. Biochem., 138 (2014) 114–121.
[25] R. Ballesteros-Garrido, R.M. Martínez, G. Rodrigo, Bacterial population control with macroscopic HKUST crystals, ACS Appl. Mater. Interfaces, 11 (2019) 19878–19883.
[26] L. Huang, J. Chen, T. Gao, M. Zhang, Y. Li, L. Dai, L. Qu, G. Shi, Reduced graphene oxide membranes for ultrafast organic solvent nanofiltration, Adv. Mater., 28 (2016) 8669–8674.
[27] A. Huang, Q. Liu, N. Wang, Y. Zhu, J. Caro, Bicontinuous zeolitic imidazolate framework ZIF-8@GO membrane with enhanced hydrogen selectivity, J. Am. Chem. Soc., 136 (2014) 14686–14689.
[28] L. Wang, N. Wang, J. Li, J. Li, W. Bian, S. Ji, Layer-by-layer self-assembly of polycation/GO nanofiltration membrane with enhanced stability and fouling resistance, Sep. Purif. Technol., 160 (2016) 123–131.
[29] S. Liu, T.H. Zeng, M. Hofmann, E. Burcombe, J. Wei, R. Jiang, J. Kong, Y. Chen, Antibacterial activity of graphite, graphite oxide, graphene oxide, and reduced graphene oxide membrane and oxidative stress, ACS Nano, 5 (2011) 6971–6980.
[30] N. Bagheri, M. Dastborhan, A. Khataee, J. Hassanzadeh, M. Kobya, Synthesis of g-C_3N_4@CuMOFs nanocomposite with superior peroxidase mimetic activity for the fluorometric measurement of glucose, Spectrochim. Acta, Part A, 213 (2019) 28–36.
[31] M. Chen, Y. Ding, Y. Liu, N. Wang, B. Yang, L. Ma, Adsorptive desulfurization of thiophene from the model fuels onto graphite oxide/metal-organic framework composites, Pet. Sci. Technol., 36 (2018) 141–147.
[32] F.N. Azad, M. Ghaedi, K. Dashtian, S. Hajati, V. Pezeshkpour, Ultrasonically assisted hydrothermal synthesis of activated carbon-HKUST-1-MOF hybrid for efficient simultaneous ultrasound-assisted removal of ternary organic dyes and antibacterial investigation: taguchi optimization, Ultrason. Sonochem., 31 (2016) 383–393.
[33] Y. Liu, M. Zhu, M. Chen, L. Ma, B. Yang, L. Li, W. Tu, A polydopamine-modified reduced graphene oxide (rGO)/MOFs nanocomposite with fast rejection capacity for organic dye, Chem. Eng. J., 359 (2019) 47–57.
[34] B. Shi, Y. Li, H. Zhang, W. Wu, R. Ding, J. Dang, J. Wang, Tuning the performance of anion exchange membranes by embedding multifunctional nanotubes into a polymer matrix, J. Membr. Sci., 498 (2016) 242–253.
[35] M. Jin, X. Qian, J. Gao, J. Chen, D.K. Hensley, H.C. Ho, R.J. Percoco, C.M. Ritzi, Y. Yue, Solvent-free synthesis of CuO/HKUST-1 composite and its photocatalytic application, Inorg. Chem., 58 (2019) 8332–8338.
[36] W. Gao, Y. Ma, Y. Zhang, Q. Chen, H. Chen, B. Zhu, J. Jia, A. Huang, K. Xie, Y. Bai, Architecture & functionalization evolution of rGO affect physicomechanical properties of polyolefin/rGO composites, Compos. Part A Appl. Sci. Manuf., 107 (2018) 479–488.
[37] Y. Liu, T. Liu, L. Tian, L. Zhang, L. Yao, T. Tan, J. Xu, X. Han, D. Liu, C. Wang, Cu_2O-directed in situ growth of Au nanoparticles inside HKUST-1 nanocages, Nanoscale, 8 (2016) 19075–19085.
[38] M. Caroff, D. Karibian, J.M. Cavaillon, N.H. Cavaillon, Structural and functional analyses of bacterial lipopolysaccharides, Microbes Infect., 4 (2002) 915–926.
[39] A. van der Wal, W. Norde, A.J.B. Zehnder, J. Lyklema, Determination of the total charge in the cell walls of Gram-positive bacteria, Colloids Surf., B, 9 (1997) 81–100.
[40] A.L. Lewis, Phosphorylcholine-based polymers and their use in the prevention of biofouling, Colloids Surf., B, 18 (2000) 261–275.
[41] K. Hirota, K. Murakami, K. Nemoto, Y. Miyake, Coating of a surface with 2-methacryloyloxyethyl phosphorylcholine (MPC) co-polymer significantly reduces retention of human pathogenic microorganisms, FEMS Microbiol. Lett., 248 (2005) 37–45.
[42] S.F. Seyedpour, A. Rahimpour, G. Najafpour, Facile in-situ assembly of silver-based MOFs to surface functionalization of TFC membrane: a novel approach toward long-lasting biofouling mitigation, J. Membr. Sci., 573 (2019) 257–269.
[43] Y. Zhang, S. Chen, J. An, H. Fu, X. Wu, C. Pang, H. Gao, Construction of an antibacterial membrane based on dopamine and polyethylenimine cross-linked graphene oxide, ACS Biomater Sci. Eng., 5 (2019) 2732–2739.